Review of Scientific Instruments

Phased plan for the implementation of the time-resolving magnetic recoil spectrometer on the National Ignition Facility (NIF)

Cite as: Rev. Sci. Instrum. **93**, 083511 (2022); https://doi.org/10.1063/5.0100996
Submitted: 27 May 2022 • Accepted: 25 July 2022 • Published Online: 16 August 2022
Published open access through an agreement with Massachusetts Institute of Technology

J. H. Kunimune, M. Gatu Johnson, A. S. Moore, et al.

Review of Scientific Instruments ARTICLE scitation.org/journal/rsi

Phased plan for the implementation of the time-resolving magnetic recoil spectrometer on the National Ignition Facility (NIF)

Cite as: Rev. Sci. Instrum. 93, 083511 (2022); doi: 10.1063/5.0100996
Submitted: 27 May 2022 • Accepted: 25 July 2022 •
Published Online: 16 August 2022

J. H. Kunimune,[1,a)] M. Gatu Johnson,[1] A. S. Moore,[2] C. A. Trosseille,[2] T. M. Johnson,[1] G. P. A. Berg,[3] A. J. Mackinnon,[2] J. D. Kilkenny,[2] and J. A. Frenje[1]

AFFILIATIONS

[1] MIT PSFC, Cambridge, Massachusetts 02139, USA
[2] LLNL, Livermore, California 94550, USA
[3] Department of Physics and Astronomy, Notre Dame, Indiana 46556, USA

Note: This paper is part of the Special Topic on Proceedings of the 24th Topical Conference on High-Temperature Plasma Diagnostics.
[a)]**Author to whom correspondence should be addressed:** kunimune@mit.edu

ABSTRACT

The time-resolving magnetic recoil spectrometer (MRSt) is a transformative diagnostic that will be used to measure the time-resolved neutron spectrum from an inertial confinement fusion implosion at the National Ignition Facility (NIF). It uses a CD foil on the outside of the hohlraum to convert fusion neutrons to recoil deuterons. An ion-optical system positioned outside the NIF target chamber energy-disperses and focuses forward-scattered deuterons. A pulse-dilation drift tube (PDDT) subsequently dilates, un-skews, and detects the signal. While the foil and ion-optical system have been designed, the PDDT requires more development before it can be implemented. Therefore, a phased plan is presented that first uses the foil and ion-optical systems with detectors that can be implemented immediately—namely CR-39 and hDISC streak cameras. These detectors will allow the MRSt to be commissioned in an intermediate stage and begin collecting data on a reduced timescale, while the PDDT is developed in parallel. A CR-39 detector will be used in phase 1 for the measurement of the time-integrated neutron spectra with excellent energy-resolution, necessary for the energy calibration of the system. Streak cameras will be used in phase 2 for measurement of the time-resolved spectrum with limited spectral coverage, which is sufficient to diagnose the time-resolved ion temperature. Simulations are presented that predict the performance of the streak camera detector, indicating that it will achieve excellent burn history measurements at current yields, and good time-resolved ion-temperature measurements at yields above 3×10^{17}. The PDDT will be used for optimal efficiency and resolution in phase 3.

I. INTRODUCTION

At the National Ignition Facility (NIF),[1] inertial confinement fusion (ICF) implosions are routinely diagnosed using neutron spectroscopy.[2] Current detectors at the NIF are used to measure time-integrated spectra, from which the time-integrated, burn-weighted ion temperature T_i, areal density ρR, and yield Y_n are inferred.[3–5] However, to fully understand the evolution of an implosion, time-resolved measurements of $T_i(t)$, $\rho R(t)$, and $Y_n(t)$ are needed. The time-resolving magnetic recoil spectrometer (MRSt) is a novel diagnostic that is being implemented at the NIF for time-resolved measurements of the neutron spectrum from an inertial confinement fusion (ICF) implosion, from which $T_i(t)$, $\rho R(t)$, and $Y_n(t)$ will be inferred.[6] Key parameters, such as the burn width, burn

skewness, burn kurtosis, dT_i/dt at bang time (BT), and $d\rho R/dt$ at BT, will provide valuable insight into the dynamics of the ICF implosion and, in particular, the effects of alpha heating, low-mode asymmetry, and mix, as well as proximity to ignition.[7] MRSt has been identified by the National Diagnostic Working Group as one of the key new diagnostics that will transform how ICF implosions are diagnosed.[8]

The MRSt concept, shown in Fig. 1, expands on the existing magnetic recoil spectrometer (MRS).[3] A fraction of the fusion neutrons emitted from an ICF implosion interacts with a deuterated foil mounted on the hohlraum 4 mm away from the implosion, generating recoil deuterons.[9] The forward-scattered deuterons are selected by an aperture located 6 m from the implosion. Deuterons with energies between 10.7 and 14.2 MeV are subsequently energy-dispersed across a 40 cm focal plane by an ion-optical system.[10]

The MRSt can be configured to account for different expected yields.[7,10] For low yields, a larger conversion foil and wider entrance will be used to increase the detection efficiency at the expense of time and energy resolution. For high yields, a smaller foil and narrower entrance will be used to improve time and energy resolution at the expense of efficiency. The three configurations that will be used are summarized in Table I.

The back-end component of the MRSt system is the detector. The final version of the MRSt will use a pulse-dilation drift tube (PDDT)[11] with a CsI cathode positioned at the focal plane of the ion optics. In the CsI cathode, recoil deuterons will be converted to secondary electrons. A time- and space-varying electric field will dilate and un-skew the secondary electron distribution. The signal will be subsequently amplified by a microchannel plate and detected by an array of anodes.[11] With the PDDT, MRSt will obtain novel measurements that enable studies of alpha heating and different failure modes in an ICF implosion with unprecedented precision.[7]

While the conversion foil and ion optics have been designed,[9,10] further research and development is needed to implement the PDDT. Therefore, a phased approach is being planned for the implementation of the MRSt system. In phase 1, a CR-39 detector will be used to obtain a time-integrated spectrum to calibrate the ion optics. In phase 2, two streak cameras will be used to obtain time-resolved $Y_n(t)$ and $T_i(t)$ measurements. In phase 3, the PDDT will be implemented to obtain high-precision $Y_n(t)$, $T_i(t)$, and $\rho R(t)$.

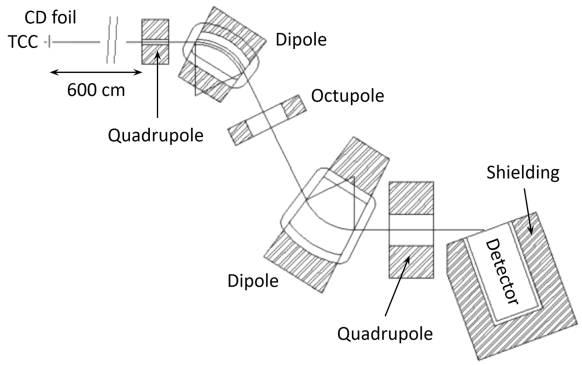

FIG. 1. A schematic layout of the MRSt system. The foil attached to the hohlraum near target chamber center (TCC) will convert fusion neutrons to recoil deuterons. Forward-scattered deuterons will then be selected by an entrance aperture 6 m away and dispersed and focused by an ion-optical system described by Berg *et al.*[10] The detector will consist of a CR-39 detector in phase 1, streak cameras in phase 2, and a pulse-dilation drift tube (PDDT) in phase 3.[11] Reproduced from Kunimune *et al.*, Rev. Sci. Instrum. **92**(3), 033514 (2021) with the permission of AIP Publishing.

TABLE I. Properties of the three MRSt configurations, as well as their performance metrics. The resolutions given are the FWHMs of the ion-optic response function, and the ion-optic efficiency is the fraction of neutrons from the implosion that generate a recoil deuteron that passes through the aperture. These numbers do not account for the detector, which may impact both resolution and efficiency.

Configuration	Low-eff.	Medium-eff.	High-eff.
Foil thickness (μm)	25	40	90
Foil radius (μm)	100	200	300
Aperture width (mm)	2	3	5
Time resolution (ps)	37.9	59.1	84.8
Energy resolution (keV)	201	322	737
Efficiency (10^{-13})	0.40	3.8	32

II. PHASE 1: CR-39 FOR TIME-INTEGRATED MEASUREMENTS

In phase 1, the MRSt will be implemented with a CR-39 detector to calibrate the ion optics. CR-39 is a solid-state detector in which charged particles leave tracks of chemical damage. The diameter of these tracks can be increased by etching the CR-39 in NaOH until they are visible under a microscope.[12] CR-39 has excellent spatial resolution and can cover an arbitrarily large collection area. It also has 100% efficiency for detecting recoil deuterons. This makes it ideal for measuring a time-integrated neutron spectrum. In this phase, the MRSt will be conceptually similar to the existing MRS.[3]

This phase will be used to characterize and calibrate the ion optics of the MRSt system. One way to do this is using americium-241 and radium-226 alpha sources. These sources produce alpha particles at energies between 4 and 8 MeV, which can be transported through the ion optics to establish the relationship between particle energy and position at the focal plane. This is much the same as the procedure used to calibrate the charged particle spectrometer at OMEGA.[13]

III. PHASE 2: STREAK CAMERAS FOR TIME-RESOLVED MEASUREMENTS

In phase 2, the CR-39 detector will be replaced with two streak cameras. A streak camera is a time- and space-resolving detector that can measure various kinds of radiation.[14,15] The radiation is selected by a narrow slit and then converted to secondary electrons in a cathode. The electrons are subsequently accelerated and focused through an electron-optic streak tube onto a CCD camera, which records them. The time resolution is provided by the electron-optics, which sweep the electron beam in the direction perpendicular to the slit.

Because streak cameras are routinely used in various diagnostics at the NIF,[14] this detector option can be implemented immediately upon the completion of phase 1. This makes streak cameras an excellent temporary detector to provide time-resolved measurements of T_i while the PDDT is being developed.

The hDISC streak camera will be used for the MRSt.[16] It uses a CsI cathode, which is usually used to detect x rays, but will respond similarly to recoil deuterons.[17] The cameras will be positioned with their slits along the focal plane, where the streak cameras' spatial resolution along the slit provides energy resolution of the deuteron spectrum.

Work is ongoing to identify the slit sizes, slit positions, and focal plane tilt angle that optimize the efficiency and resolution of the phase-2 MRSt system. For now, a point design has been identified to characterize the capabilities of the streak camera detector.

The point design utilizes two slits with 26 mm long and 0.4 mm wide active areas. The detection efficiency of each streak camera is limited by the area of the slit relative to the spatial extent of the recoil deuterons incident onto the focal plane, which varies with energy, as illustrated in Fig. 2.

With one slit positioned over the point of vertical focus at 12.0 MeV and the other over the location of the primary peak at 12.5 MeV, the achieved efficiency is 0.12 times the ion-optic efficiency (see Table I). To compensate for this reduction, the high-efficiency configuration will be used. The reduction in detection efficiency means that phase-2 MRSt will not diagnose ρR. The ρR must be inferred from the downscattered portion of the spectrum, which produces too few deuterons over too large an area to be measured with appreciable statistics through a streak camera slit.

Synthetic data analysis was used to validate that the phase-2 MRSt can obtain sufficiently precise information about $Y_n(t)$ and $T_i(t)$, similar to the work described by Kunimune *et al.*[7] A synthetic neutron spectrum based on the $Y_n(t)$, $T_i(t)$, and $\rho R(t)$ output from a HYDRA simulation was used in this analysis.[18] The primary peak was assumed to be Gaussian, with a width dependent on T_i alone.[2] The spectrum was scaled up or down to account for different yield levels. Future analysis will also vary the spectral shape based on different scenarios. To model the response of the foil and ion-opics, Monte Carlo simulations were performed in which recoil deuterons are generated at random locations in the foil, and subsequently allowed to propagate through the ion optics according to a COSY INFINITY model of the MRSt.[19]

To model the response of the streak cameras, the image of the slit on the CCD is approximated as a true-size projection moving at a constant speed, assumed to be 5.6 mm/ns. This means that the width of the slit degrades the time resolution by $\Delta t = 0.4\ \text{mm}/(5.6\ \text{mm/ns}) = 72$ ps. Combined with the 85 ps FWHM of the ion-optics response function in the high-efficiency configuration, this results in a total time response width of about 111 ps.

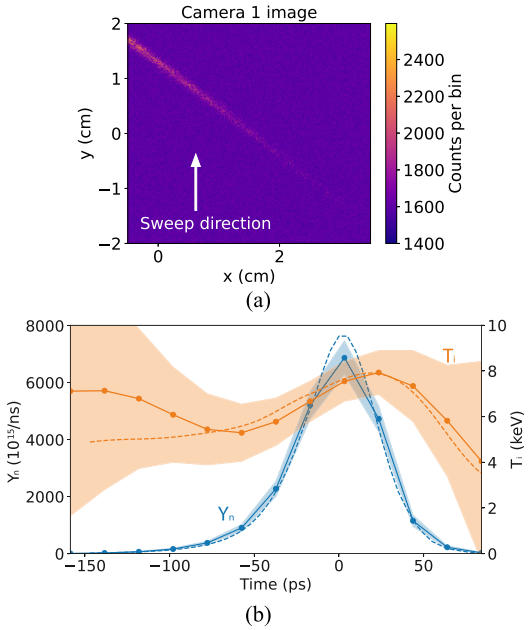

FIG. 3. Phase-2 MRSt synthetic data to illustrate the performance of the system. A total neutron yield of 4×10^{17} was used for this simulation. (a) A synthetic streak image for the higher-energy slit. The *x*-direction corresponds to direction along the slit, and the ion-optics provide energy resolution along this axis. The streak camera sweeps the electron beam upward to provide time resolution along the *y*-axis. The signal is heavily skewed due to the well-known relationship between deuteron energy and time-of-flight. The vertical extent of the image corresponds to 4.5 ns, which is set by the time-of-flight difference between the highest and lowest measured deuteron energies. (b) Inferred $Y_n(t)$ and $T_i(t)$ from the synthetic streak image. The solid lines represent the inference, the shaded regions represent the uncertainty of the inference, and the dashed curves represent the original values used to generate the data.

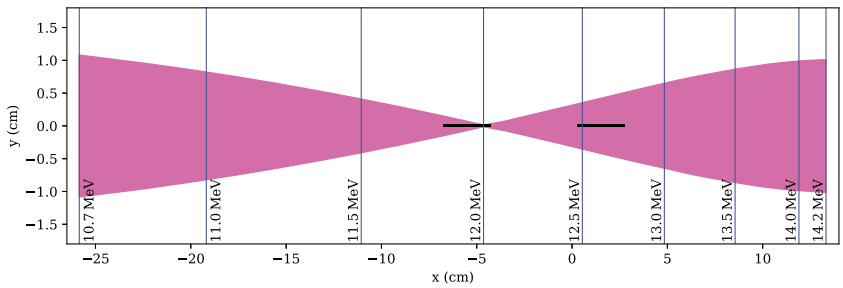

FIG. 2. The size and location of the streak camera slits relative to the distribution of recoil deuterons at the focal plane. The black bars at $x = -5.5$ and $x = 1.5$ represent the streak camera slits. The shaded region indicates where recoil deuterons are incident. The vertical lines indicate the *x* values corresponding to different deuteron energies. The 10.7 MeV deuterons strike the detector 40 cm away from the 14.2 MeV deuterons.[10] Because the ion optics are focused in the dispersive (x) direction and not in the vertical (y) direction, mono-energetic deuterons are incident in vertical bands up to 2 cm long; the dependence of the band length with energy gives rise to the bowtie-like shape of the signal distribution at the focal plane. At the center of the bowtie, where 12 MeV deuterons are incident, the signal is focused in both directions. The primary neutron peak at 14.1 MeV produces recoil deuterons at about 12.5 MeV.

A flat noisy background of 100 ± 10 counts per 25 μm square is added on top of the streak signal. This is a conservative estimate based on the number of fusion neutrons that will collide with the detector during a high-yield shot. This number can be reduced by accounting for shielding.

The Monte Carlo simulations are used to produce synthetic streak images, like the one shown in Fig. 3(a), as well as time-corrected deuteron histograms in time and energy, like the one shown in Fig. 3(b). These histograms are analyzed using a forward-fit technique where perfect knowledge of the instrument response is assumed, and $T_i(t)$ and $Y_n(t)$ are inferred, as shown in Fig. 3(c). From those curves, key parameters, such as the burn width and dT_i/dt at BT, are extracted. By repeating this analysis for many different random seeds and many different yields, the accuracy with which the phase-2 MRSt will measure those parameters is estimated.

As this study neglects important sources of systematic error, such as uncertainty in the instrument response function, it provides a lower-bound on the actual error that can be expected. Analysis of the magnitude of these systematic errors is a work in progress.

The results of this study are shown in Fig. 4 and Table II and compared to the top-level physics requirements for MRSt. With the MRSt in the high-efficiency configuration, the phase-2 system will meet the top-level physics requirements for burn width, burn skewness, and burn kurtosis at current yield levels. It will also help to constrain the T_i and dT_i/dt at bang time with modest error bars. When yields are routinely above 3×10^{17}, the phase-2 MRSt will meet the T_i and dT_i/dt top-level physics requirements needed to probe the effects of alpha heating, low-mode asymmetry, and mix in ICF implosions at current yields.

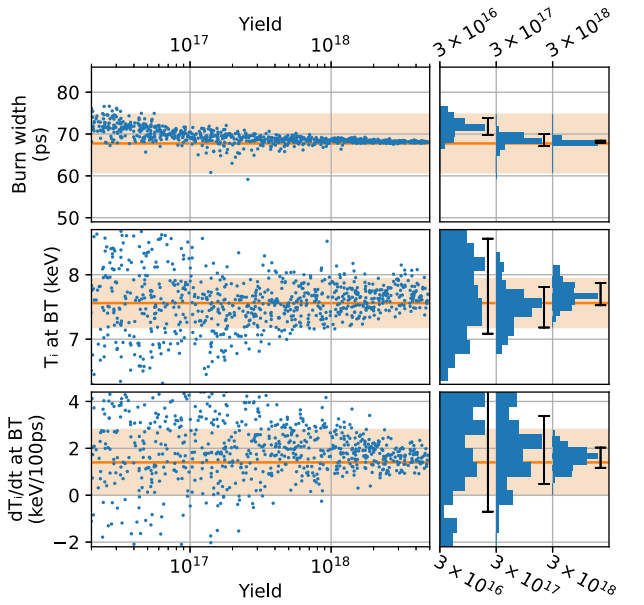

FIG. 4. Monte Carlo simulated performance of the phase-2 MRSt at yields from 2×10^{16} to 5×10^{18}. Each data point represents a value inferred from one synthetic spectrum. The horizontal line indicates the true value used to generate the synthetic data, and the shaded region represents the top-level physics requirement. Histograms on the right show the vertical distribution of the blue points at the three yield values examined in Table II, and black lines show their standard deviations. Where the points appear higher than the dashed line, as in the burn-width plot, it means that the measurement is systematically overestimated (this is due to the nature of the initial guess of the fitting algorithm, which biases the result when the yield is low).

TABLE II. Measurement capabilities of the phase-2 MRSt in the high-efficiency configuration. Each given value is the error of the measurement at one yield. The error is defined as the root-mean-square of the difference between the synthetic inferences and the true value (essentially the standard deviation of the data points in Fig. 4). The required accuracies are given on the right for reference.

Yield	3×10^{16}	3×10^{17}	3×10^{18}	Req.
Burn width (ps)	±4.5	±1.7	±0.50	±7
Burn skewness	±0.20	±0.10	±0.025	±0.3
Burn kurtosis	±0.67	±0.31	±0.10	±3
T_i at BT (keV)	±0.78	±0.32	±0.22	±0.4
dT_i/dt at BT (keV/ns)	±33	±15	±4.8	±14

IV. PHASE 3: PULSE-DILATION DRIFT TUBE

In the phase-3 implementation of MRSt, a PDDT will be incorporated for optimal resolution and efficiency. The efficiency of the PDDT for detecting recoil deuterons is nearly 100%,[17,20] and its time resolution is 20 ps.[11] Since the phase-3 MRSt will be used to measure the full deuteron spectrum from 10.7 to 14.2 MeV, it will also provide the first time-resolved measurements of $\rho R(t)$.

Synthetic data analysis was performed based on the phase-3 MRSt.[7] These data are generated with the medium-efficiency configuration, as the higher efficiency of the PDDT allows us to use

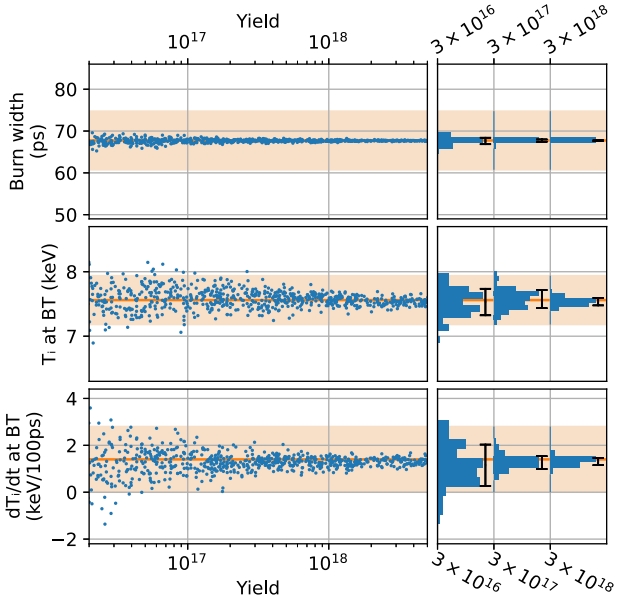

FIG. 5. Monte Carlo simulated performance of the phase-3 MRSt at yields from 2×10^{16} to 5×10^{18}. Compare to Fig. 4.

TABLE III. Measurement capabilities of the phase-3 MRSt in the medium-efficiency configuration. Compare to Table II.

Yield	3×10^{16}	3×10^{17}	3×10^{18}	Req.
Burn width (ps)	±0.79	±0.28	±0.11	±7
Burn skew	±0.072	±0.021	±0.016	±0.3
Burn kurtosis	±0.35	±0.084	±0.037	±3
T_i at BT (keV)	±0.21	±0.14	±0.063	±0.4
dT_i/dt at BT (keV/ns)	±9.2	±3.1	±1.8	±14
ρR at BT (g/cm^2)	±0.047	±0.024	±0.016	±0.07
Peak ρR (g/cm^2)	±0.11	±0.054	±0.031	±0.07

finer resolution while still obtaining reasonable statistics. The analysis is shown in Fig. 5 and Table III, and it indicates that the phase-3 MRSt system will meet the top-level physics requirements for measurements of burn width, burn skewness, burn kurtosis, $T_i(t)$, and $\rho R(t)$ at current yields.

The PDDT has been conceptually designed and tested,[11,17,20–22] and can be developed in parallel with the phase-1 and phase-2 MRSt operation. Once it is completed, it will replace the streak cameras and serve as the permanent detector for the MRSt.

V. CONCLUSION

The MRSt is a transformative diagnostic tool that will provide the first ever time-resolved measurement of the neutron spectrum generated from an ICF implosion. A phased approach is described for implementation of the system on NIF. In phase 1, a CR-39 detector will be used for measurement of a time-integrated spectrum, which will be used to calibrate the ion optics. In phase 2, two streak cameras will be positioned next to each other to obtain time-resolved measurements of $Y_n(t)$ and $T_i(t)$. Synthetic data have been generated and analyzed at a variety of yields to predict the performance of the phase-2 system. Finally, in phase 3, a PDDT will be implemented to provide excellent resolution and detection efficiency while also enabling time-resolved measurements of $\rho R(t)$. At each phase, the MRSt will advance our understanding of the dynamics that govern an ICF implosion.

ACKNOWLEDGMENTS

This work was supported, in part, by the U.S. Department of Energy NNSA MIT Center-of-Excellence under Contract No. DE-NA0003868 and Lawrence Livermore National Laboratory under Contract No. B635598.

This report was prepared as an account of work sponsored by an agency of the United States Government. Neither the United States Government nor any agency thereof, nor any of their employees, makes any warranty, express or implied, or assumes any legal liability or responsibility for the accuracy, completeness, or usefulness of any information, apparatus, product, or process disclosed, or represents that its use would not infringe privately owned rights. Reference herein to any specific commercial product, process, or service by trade name, trademark, manufacturer, or otherwise does not necessarily constitute or imply its endorsement, recommendation, or favoring by the United States Government or any agency thereof. The views and opinions of authors expressed herein do not necessarily state or reflect those of the United States Government or any agency thereof.

This document has been reviewed for release as document LLNL-PROC-835919.

AUTHOR DECLARATIONS

Conflict of Interest

The authors have no conflicts to disclose.

Author Contributions

J. H. Kunimune: Investigation (lead); Writing – original draft (lead); Writing – review & editing (equal). **M. Gatu Johnson**: Investigation (supporting); Supervision (equal); Writing – review & editing (equal). **A. S. Moore**: Investigation (supporting). **C. A. Trosseille**: Investigation (supporting); Writing – review & editing (equal). **T. M. Johnson**: Resources (equal). **G. P. A. Berg**: Investigation (supporting); Writing – review & editing (equal). **A. J. Mackinnon**: Supervision (equal). **J. D. Kilkenny**: Supervision (equal). **J. A. Frenje**: Supervision (equal); Writing – review & editing (equal).

DATA AVAILABILITY

The data that support the findings of this study are available from the corresponding author upon reasonable request.

REFERENCES

[1] G. H. Miller *et al.*, Nucl. Fusion **44**(12), S228–S238 (2004).
[2] J. A. Frenje, Plasma Phys. Control. Fusion **62**(2), 023001 (2020).
[3] D. T. Casey *et al.*, Rev. Sci. Instrum. **84**(4), 043506 (2013).
[4] J. A. Frenje *et al.*, Phys. Plasmas **17**(5), 056311 (2010).
[5] R. Hatarik *et al.*, J. Appl. Phys. **118**(18), 184502 (2015).
[6] J. A. Frenje *et al.*, Rev. Sci. Instrum. **87**(11), 11D806 (2016).
[7] J. H. Kunimune *et al.*, Rev. Sci. Instrum. **92**(3), 033514 (2021).
[8] J. Kilkenny, The ICF National Diagnostic Plan, September 2018, Technical Report No. LLNL-TR-759117, National Diagnostics Working Group, 2018.
[9] C. E. Parker *et al.*, Rev. Sci. Instrum. **89**(11), 113508 (2018).
[10] G. P. A. Berg *et al.*, Rev. Sci. Instrum. **93**(3), 033505 (2022).
[11] T. J. Hilsabeck *et al.*, Rev. Sci. Instrum. **87**(11), 11D807 (2016).
[12] B. Lahmann *et al.*, Rev. Sci. Instrum. **91**(5), 053502 (2020).
[13] P. J. Adrian *et al.*, "*In situ* calibration of charged particle spectrometers on the OMEGA Laser Facility using Am-241 and Ra-226 sources," Rev. Sci. Instrum. (submitted).
[14] J. R. Kimbrough *et al.*, Rev. Sci. Instrum. **72**(1), 748 (2001).
[15] Y. P. Opachich *et al.*, Rev. Sci. Instrum. **83**(12), 125105 (2012).
[16] A. G. MacPhee *et al.*, "Performance of a radiation-hardened x-ray streak camera at LLNL's National Ignition Facility," Rev. Sci. Instrum. (submitted).
[17] C. W. Wink *et al.*, Rev. Sci. Instrum. **87**(11), 11D808 (2016).
[18] S. H. Langer *et al.*, in *High Performance Computing for Computational Science—VECPAR 2014*, edited by M. Daydé *et al.* (Springer International Publishing, Cham, 2015), pp. 173–181.
[19] K. Makino *et al.*, Nucl. Instrum. Methods Phys. Res., Sect. A **427**(1), 338 (1999).
[20] C. E. Parker *et al.*, Rev. Sci. Instrum. **90**(10), 103306 (2019).
[21] C. W. Wink, M.S. thesis, Massachusetts Institute of Technology, 2017.
[22] A. J. Sandberg, M.S. thesis, Massachusetts Institute of Technology, 2019.